

A geometric invariant for the study of planar curves and its application to spiral tip meander.

Copyright © 2016 Scott Hotton
email: scotton@sdf.org

Contents

1 Introduction

2 The geometric invariant $|\check{\kappa}|$

3 Conservative examples

4 Dissipative examples

5 Conclusion

1 Introduction

2 The geometric invariant $|\check{\kappa}|$

Lets begin by reviewing some differential geometry of planar curves. We let t stand for time and we denote the position of the moving point at time t by $(x(t), y(t))^T$. There are two important functions associated to twice differentiable planar curves, their speed and local curvature (more commonly referred to as just curvature). We denote the speed by $v(t)$ and the local curvature by $\kappa(t)$. Also we will denote the direction of the velocity by $\theta \in \mathbf{S}$. Roughly speaking the local curvature tells us how fast θ is changing at a point of the curve.

If the velocity is defined and never equal to $(0, 0)^T$ the curve is said to be *immersed*. If $v(t) \equiv 1$ the curve is said to have *unit speed*. In theory immersed curves can be reparameterized to have unit speed. This is done using the concept of arc length. A closed form for arc length can sometimes be obtained from the integral

$$s(t) = \int_0^t v(\tau) d\tau = \int_0^t \sqrt{\dot{x}(\tau)^2 + \dot{y}(\tau)^2} d\tau$$

although in actual practice its often not feasible to find an anti-derivative for $\sqrt{\dot{x}(\tau)^2 + \dot{y}(\tau)^2}$ because of the square root. In any case local curvature has been defined as $\kappa(s) = d\theta/ds$.

Although its usually not feasible to compute $\kappa(s)$ it is usually not too difficult to compute

$$\kappa(s(t)) = \frac{\dot{x}(t)\ddot{y}(t) - \dot{y}(t)\ddot{x}(t)}{(\dot{x}(t)^2 + \dot{y}(t)^2)^{3/2}}$$

and this is often sufficient for many purposes. Its common practice to write $\kappa(t)$ for $\kappa(s(t))$ and we will use this convention here.

Roughly speaking the total curvature of a curve is how much θ changes over the whole curve. Historically total curvature has been defined as the integral of local curvature. This had the drawback of making it seem that local curvature needed to be defined in order for total curvature to be defined. Fox and Milnor realized however that total curvature is a meaningful concept for all geometric curves [8, 15]. Moreover wherever local curvature is a meaningful concept it can be defined in terms of total curvature so total curvature is the more fundamental concept. Total curvature can still be computed from the integral of local curvature when local curvature is defined but this is no longer regarded as a definition of total curvature. This is now known as the Fox-Milnor theorem and it is how we will compute total curvature here.

Note that the Fox-Milnor theorem computes total curvature as the integral of $\kappa(s)$ with respect to arc length not as the integral of $\kappa(t)$ with respect to time. By the change of variables theorem

$$\int_{s_1}^{s_2} \kappa(\sigma) d\sigma = \int_{t_1}^{t_2} \kappa(\tau) v(\tau) d\tau \neq \int_{t_1}^{t_2} \kappa(\tau) d\tau$$

The integral for total curvature could be reformulated using $\dot{\theta}(t) = \kappa(t)v(t)$. However if we apply the fundamental theorem of calculus naively we might write

$$\int_{t_1}^{t_2} \dot{\theta}(\tau) d\tau = \theta(t_2) - \theta(t_1)$$

but this is only the difference between the starting direction and final direction of the velocity and it overlooks the possibility that the velocity may have undergone several complete turns during the time interval $[t_1, t_2]$. To take this possibility into consideration we define the function.

$$\varphi(t) = \theta(0) + \int_0^t \kappa(\tau)v(\tau) d\tau$$

The set of all values for θ has the topology of a circle whereas φ can take on any real number value since it is the integral of the real valued function $\kappa(t)v(t)$. We can recover θ from φ by taking its value modulo 2π . The rate of change of θ and φ are numerically equal, *i.e.* $\dot{\varphi}(t) = \dot{\theta}(t)$. By the Fox-Milnor theorem the total curvature of the curve from $t = t_1$ to $t = t_2$ is

$$\int_{t_1}^{t_2} \dot{\varphi}(\tau) d\tau = \varphi(t_2) - \varphi(t_1)$$

The *turning number* is the total curvature divided by 2π . It measures how far the tangent vector has turned over the length of the curve.

The velocity of the curve can be expressed in terms of $\varphi(t)$ as $v(t) (\cos(\varphi(t)), \sin(\varphi(t)))^T$. Given the initial point of the curve, $(x(0), y(0))^T$, we can express the point at other times as

$$\begin{pmatrix} x(t) \\ y(t) \end{pmatrix} = \begin{pmatrix} x(0) \\ y(0) \end{pmatrix} + \int_0^t v(\tau) \begin{pmatrix} \cos(\varphi(\tau)) \\ \sin(\varphi(\tau)) \end{pmatrix} d\tau \quad (2.1)$$

We now assume that the speed and curvature are defined for all $t \in \mathbf{R}$ and that they are periodic functions with a common minimal period $T > 0$. This can occur by $(x(t), y(t))^T$ having period T but this is not necessary. We call an arc within such a curve whose domain is an interval of length T a *periodic arc* of the curve. We show how to partition such curves into congruent periodic arcs below.

It follows that $\dot{\varphi}(t) = \kappa(t)v(t)$ is a periodic function with period T . The integral of a periodic function is periodic if its average value over one period is zero. And if we subtract the average value from a periodic function its integral will be periodic. So we set

$$\begin{aligned} \bar{\kappa} &= \frac{1}{T} \int_0^T v(\tau)\kappa(\tau) d\tau \\ \tilde{\varphi}(t) &= \kappa(0)v(0) + \int_0^t \kappa(\tau)v(\tau) - \bar{\kappa} d\tau \end{aligned}$$

This allows us to write $\varphi(t) = \bar{\kappa} t + \tilde{\varphi}(t)$ where $\tilde{\varphi}(t)$ has period T . We let R_ϕ stands for a rotation by ϕ radians. Even though $\varphi(t)$ is not periodic whenever $\bar{\kappa} \neq 0$ it is the case that

Lemma 1. *For all $t \in \mathbf{R}$*

$$R_{\bar{\kappa} T} \begin{pmatrix} \cos(\varphi(t)) \\ \sin(\varphi(t)) \end{pmatrix} = \begin{pmatrix} \cos(\varphi(t+T)) \\ \sin(\varphi(t+T)) \end{pmatrix}$$

Proof. After making the substitution $\varphi(t) = \bar{\kappa} t + \tilde{\varphi}(t)$ the proof is just a calculation which makes use of matrix multiplication, addition rules from trigonometry, and the fact that $\tilde{\varphi}(t)$ has period T . \square

The quantity $\bar{\kappa} T$ is the total curvature for the periodic arcs of the curve. We denote the turning number of a periodic arc by $\tilde{\kappa}$. Note this is independent of the choice of periodic arc. For any $t_0 \in \mathbf{R}$

$$\begin{aligned} \tilde{\kappa} &= \frac{\bar{\kappa} T}{2\pi} = \frac{1}{2\pi} \int_{t_0}^{t_0+T} \kappa(\tau)v(\tau) d\tau \\ &= \frac{1}{2\pi} \int_0^T \frac{\dot{x}(\tau)\ddot{y}(\tau) - \dot{y}(\tau)\ddot{x}(\tau)}{\dot{x}(\tau)^2 + \dot{y}(\tau)^2} d\tau \quad (2.2) \end{aligned}$$

An advantage of $\tilde{\kappa}$ is that, unlike arc length, it doesn't necessarily contain a radical under the integral which improves the prospects of finding an anti-derivative for use in the fundamental theorem of calculus.

Winfree coined the term “isogon contours” in his study of spiral tip meander [19]. We say here that an *isogonal curve* is a level curve of $\tilde{\kappa}$ whether $\tilde{\kappa}$ is seen as a function in the state space or as a function in the parameter space.

An *even* congruence is a congruence of the Euclidean plane which preserves the orientation of the plane. An *odd* congruence reverses the orientation of the plane. Total curvature is invariant under even congruences and turned into its negative by odd congruences. Thus the quantity $|\check{\kappa}|$ is invariant under all congruences. It gives us a geometric property of the curve. In particular we can express some of the curve's symmetries in terms of $\check{\kappa}$. Let

$$\mathcal{G}_{\check{\kappa},T} \begin{pmatrix} x(t) \\ y(t) \end{pmatrix} = \begin{pmatrix} \begin{pmatrix} x(T) \\ y(T) \end{pmatrix} - R_{2\pi\check{\kappa}} \begin{pmatrix} x(0) \\ y(0) \end{pmatrix} \\ R_{2\pi\check{\kappa}} \begin{pmatrix} x(t) \\ y(t) \end{pmatrix} \end{pmatrix} \quad (2.3)$$

When $\check{\kappa} \in \mathbf{Z}$ the rotation $R_{2\pi\check{\kappa}}$ reduces to the identity map and $\mathcal{G}_{\check{\kappa},T}$ is a translation by the vector $(x(T) - x(0), y(T) - y(0))^T$. Otherwise $\mathcal{G}_{\check{\kappa},T}$ is a rotation by $2\pi\check{\kappa}$ modulo 2π radians about the point

$$\begin{pmatrix} \bar{x} \\ \bar{y} \end{pmatrix} = \frac{1}{2\sin(\pi\check{\kappa})} R_{\pi(1/2-\check{\kappa})} \begin{pmatrix} x(T) - x(0) \\ y(T) - y(0) \end{pmatrix}$$

Theorem 2. For all $t \in \mathbf{R}$

$$\mathcal{G}_{\check{\kappa},T} \begin{pmatrix} x(t) \\ y(t) \end{pmatrix} = \begin{pmatrix} x(t+T) \\ y(t+T) \end{pmatrix}$$

Proof. Moving $(x(0), y(0))^T$ from the right hand side of (2.1) to the left hand side and applying the rotation $R_{2\pi\check{\kappa}}$ to both sides gives

$$\begin{aligned} R_{2\pi\check{\kappa}} \left(\begin{pmatrix} x(t) \\ y(t) \end{pmatrix} - \begin{pmatrix} x(0) \\ y(0) \end{pmatrix} \right) \\ = R_{2\pi\check{\kappa}} \int_0^t v(\tau) \begin{pmatrix} \cos(\varphi(\tau)) \\ \sin(\varphi(\tau)) \end{pmatrix} d\tau \\ = \int_0^t v(\tau) R_{2\pi\check{\kappa}} \begin{pmatrix} \cos(\varphi(\tau)) \\ \sin(\varphi(\tau)) \end{pmatrix} d\tau \end{aligned}$$

By Lemma 1

$$\begin{aligned} \int_0^t v(\tau) R_{2\pi\check{\kappa}} \begin{pmatrix} \cos(\varphi(\tau)) \\ \sin(\varphi(\tau)) \end{pmatrix} d\tau \\ = \int_0^t v(\tau) \begin{pmatrix} \cos(\varphi(\tau+T)) \\ \sin(\varphi(\tau+T)) \end{pmatrix} d\tau \end{aligned}$$

and since $v(t)$ has period T

$$\begin{aligned} \int_0^t v(\tau) \begin{pmatrix} \cos(\varphi(\tau+T)) \\ \sin(\varphi(\tau+T)) \end{pmatrix} d\tau \\ = \int_0^t v(\tau+T) \begin{pmatrix} \cos(\varphi(\tau+T)) \\ \sin(\varphi(\tau+T)) \end{pmatrix} d\tau \end{aligned}$$

Using the change of variables theorem with $\eta = \tau + T$ gives

$$\begin{aligned} \int_0^t v(\tau+T) \begin{pmatrix} \cos(\varphi(\tau+T)) \\ \sin(\varphi(\tau+T)) \end{pmatrix} d\tau = \\ \int_0^{t+T} v(\eta) \begin{pmatrix} \cos(\varphi(\eta)) \\ \sin(\varphi(\eta)) \end{pmatrix} d\eta - \int_0^T v(\eta) \begin{pmatrix} \cos(\varphi(\eta)) \\ \sin(\varphi(\eta)) \end{pmatrix} d\eta \end{aligned}$$

Therefore

$$R_{2\pi\check{\kappa}} \begin{pmatrix} x(t) \\ y(t) \end{pmatrix} - R_{2\pi\check{\kappa}} \begin{pmatrix} x(0) \\ y(0) \end{pmatrix} = \begin{pmatrix} x(t+T) \\ y(t+T) \end{pmatrix} - \begin{pmatrix} x(T) \\ y(T) \end{pmatrix}$$

which can be rearranged to give the theorem. \square

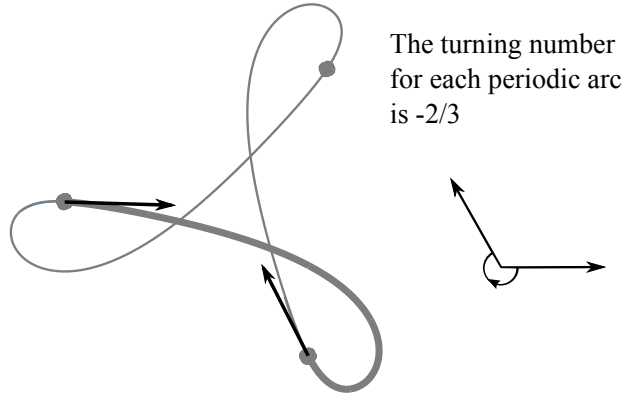


Figure 1: A curve with $\check{\kappa} = -2/3$. The curve is partitioned into three periodic arcs. The tangent vector rotates by minus two thirds of a turn from the starting point of a periodic arc to its final point. The tangent vector rotates by minus two whole turns along the entire closed curve so its Whitney turning number is -2 . The curve has no reflectional symmetry and its full symmetry group is generated by $\mathcal{G}_{-2/3,T}$.

We can arbitrarily pick any point on the curve, $(x(t_1), y(t_1))^T$, and apply $\mathcal{G}_{\check{\kappa},T}$ to it to get the point $(x(t_1+T), y(t_1+T))^T$. The portion of the curve between these two points is a periodic arc. We can apply $\mathcal{G}_{\check{\kappa},T}$ to this periodic arc to get an adjacent periodic arc and so on. We can apply the inverse of $\mathcal{G}_{\check{\kappa},T}$ to get the rest of the curve on the other side of $(x(t_1), y(t_1))^T$. In this way we can partition the curve into periodic arcs starting from any point. A simple example is shown in figure 1.

The quantity $\tilde{\kappa}$ is like the Whitney turning number [17] for closed curves except the Whitney turning number is a topological invariant whereas $\tilde{\kappa}$ is a geometric invariant. Also the value of $\tilde{\kappa}$ can be any real number whereas the Whitney turning number must be an integer. When $\tilde{\kappa}$ is a non-integral rational number p/q (p, q coprime) there is a close relationship between the two quantities. A periodic arc will return to itself after being rotated q times by $\mathcal{G}_{p/q, T}$. This implies the image of the curve is closed and that the Whitney turning number of its image is p . Conversely given a closed curve with Whitney turning number p and rotational symmetry by p/q of a turn the curve can be partitioned into q arcs with total turning number p/q . This is illustrated in figure 1.

3 Conservative examples

Example 1 - Epicyclic motion

Epicyclic motion was an ancient Greek model for our solar system¹. It was a fair approximation for the motion of the planets as seen in the Earth's rest frame but of course it has long since been superseded by Heliocentric models.

Epicyclic motion is formed by combining two rotary motions. A point on a circle, called the *deferent*, revolves with a constant angular velocity ω_1 . At each moment in time the revolving point is the center for another circle called the *epicycle* which spins about its center with constant angular velocity ω_2 . A chosen point on the epicycle, that we will call the *tracing point*, stood for the location of a planet (see figure 2). The orbit of a planet was represented by the curve generated by the tracing point.

At any moment in time the location of the tracing point can be expressed as the sum of two vectors: a position vector for the location of the center of the epicycle relative to the center of the deferent and a position vector for the location of the tracing point relative to the center

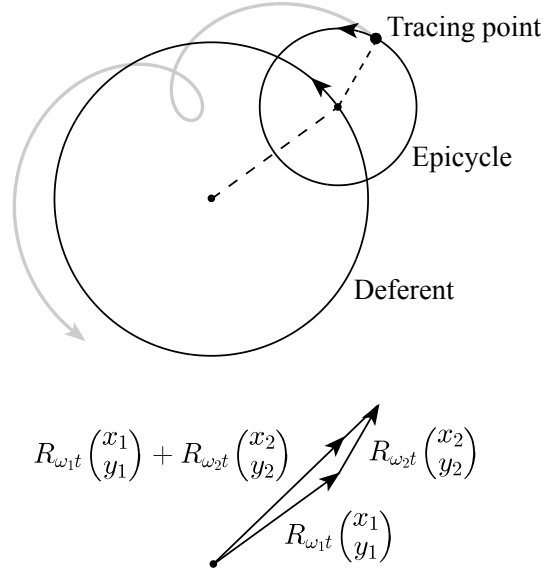


Figure 2: Epicyclic motion is the spin of the epicycle as its center revolves about the center of the deferent. It can be expressed as the sum of two vectors which turn with fixed angular velocities.

of the epicycle. We denote these two vectors at time $t = 0$ as $(x_1, y_1)^T$ and $(x_2, y_2)^T$ respectively. Figure 2 presents a simple time parametrization for curves traced out by epicyclic motion.

Epicyclic motion can be generated by projecting the orbits for a pair of uncoupled harmonic oscillators. Harmonic oscillators are conservative systems. In this case the dynamics can be obtained from the Hamiltonian

$$H(x_1, y_1, x_2, y_2) = -\frac{1}{2} (\omega_1 (x_1^2 + y_1^2) + \omega_2 (x_2^2 + y_2^2))$$

Because of the symmetry of this Hamiltonian it is arbitrary which pair of variables, x_1, x_2 or y_1, y_2 , are regarded as the positions and which are regarded as the momenta. The choice only affects the direction the system moves along the orbits. We choose x_1, x_2 to be the position variables and y_1, y_2 to be conjugate momenta. Each $(x_j, y_j)^T$ pair moves with angular frequency ω_j along a circle in the state space.

Projecting $(x_1, y_1, x_2, y_2)^T$ to the pair of position variables, $(x_1, x_2)^T$, gives us Lissajous curves. We will consider Lissajous curves only briefly. This will occur in the following example on the spherical pendulum. To obtain epicyclic motion

¹Prominent figures in the development of this model were Apollonius, Hipparchus, and Ptolemy. In Ptolemy's version the center was offset from the Earth but this did not change the shape of the curve in the Earth's rest frame.

from uncouple harmonic oscillators we instead project $(x_1, y_1, x_2, y_2)^T$ to $(x_1 + y_1, x_2 + y_2)^T$.

We set $r_j = \|(x_j, y_j)^T\|$ for $j = 1, 2$. For all $t \in \mathbf{R}$ we have

$$|r_1 - r_2| \leq \|(x(t), y(t))^T\| \leq r_1 + r_2$$

We call $|r_1 - r_2|$ the *minimum radius* and $r_1 + r_2$ the *maximum radius*. The curve attains its minimum radius when $R_{\omega_1 t}((x_1, y_1)^T)$ and $R_{\omega_2 t}((x_2, y_2)^T)$ point in opposite directions and it attains its maximum radius when they point in the same direction. By suitably shifting time we can suppose, without loss of generality, that at $t = 0$ the vectors point in the same direction. This simplifies the time parameterization of the curve to:

$$\begin{pmatrix} x(t) \\ y(t) \end{pmatrix} = R_{\omega_1 t} \begin{pmatrix} r_1 \\ 0 \end{pmatrix} + R_{\omega_2 t} \begin{pmatrix} r_2 \\ 0 \end{pmatrix} \quad (3.1)$$

If $\omega_1 = \omega_2$ then the vectors $R_{\omega_1 t}(r_1, 0)^T$, $R_{\omega_2 t}(r_2, 0)^T$ will continue to point in the same direction and the tracing point will travel in a circle. Also if $\omega_1 = 0$ or $\omega_2 = 0$ the tracing point will travel in a circle so in this section we assume that $\omega_1 \omega_2 (\omega_2 - \omega_1) \neq 0$. Furthermore, for the purpose of comparing these curves to the curves generate by spiral tip meander in section 4, we will assume $\omega_1 > 0$ which is to say the epicycle revolves anticlockwise.

Since $\omega_1 \neq \omega_2$ the vectors $R_{\omega_1 t}(r_1, 0)^T$, $R_{\omega_2 t}(r_2, 0)^T$ will alternately point in the same and opposite directions. The condition that they point in the same or opposite direction is equivalent to

$$\|(\cos(\omega_1 t), \sin(\omega_1 t), 0) \times (\cos(\omega_2 t), \sin(\omega_2 t), 0)\| = \sin((\omega_2 - \omega_1)t) = 0$$

Thus configurations for the deferent, epicycle, and tracing point which are congruent to the initial condition occur with a periodicity of $T = 2\pi/|\omega_2 - \omega_1|$. It can be checked that this is the common minimal period for $v(t)$ and $\kappa(t)$. So we can apply the theory from the previous section to epicyclic motion.

The curves generated by the tracing point are not properly called epicycles. These curves have names based on a different construction method.

They can be constructed as roulettes, *i.e.* by one curve rolling without slipping along another curve. One of the simplest non-trivial roulettes is generated by a point on a disk rolling without slipping along a line. These are called *trochoids*.

The curves generated by epicyclic motion can be generated by a circular disc rolling without slipping along another circular disc. This construction method was perhaps originally conceived of by Dürer in 1525 and then again by the astronomer Rømer in 1624. These curves have been studied by many mathematicians since.

For some purposes it is useful to allow the tracing point to be outside of the rolling disc. We can treat the union of the rolling disc and the tracing point as a single rigid body even when their union does not form a connected set. This is done by applying the same motion of the rolling disc to the tracing point regardless of where the tracing point happens to be. And since we are allowing the tracing point to be outside of the rolling disc, we can dispense with the disc's interior in the definitions and just work with a pair of circles, one fixed and one rolling along other.

The pair of circles are required to intersect in exactly one point. When they intersect in exactly one point they have the same tangent line at the contact point, hence the circles are said to be tangent to each other. If neither circle is inside the other then they are said to be externally tangent. Otherwise they are said to be internally tangent. If the fixed and rolling circles are externally tangent then the curve generated by the tracing point is called an *epitrochoid*. If the fixed circle is outside of the rolling circle then the curve is called a *hypotrochoid*. If the fixed circle is inside of the rolling circle then the curve is called a *peritrochoid*.

If the tracing point is inside of the rolling circle then the hypotrochoid, epitrochoid, or peritrochoid is said to be *curtate*. If the tracing point is outside of the rolling circle then the hypotrochoid, epitrochoid, or peritrochoid is said to be *prolate*². If the tracing point is on the

²Some authors reverse the meaning of curtate and prolate, *e.g.* [4]

rolling circle then the hypotrochoid, epitrochoid, or peritrochoid is called a *hypocycloid*, *epicycloid*, or *pericycloid* respectively

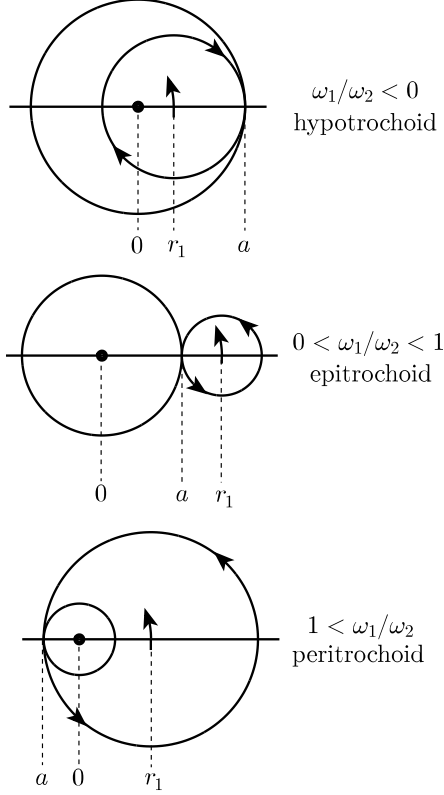


Figure 3: Three configurations for the fixed and rolling circles. We assume the rolling circles revolve anti-clockwise as indicated by the arrows at their centers. This causes the rolling circle to turn clockwise for hypotrochoids and anti-clockwise for epitrochoids and peritrochoids as indicated by the arrows on the rolling circles.

It is useful to have one term which encompasses hypotrochoids, epitrochoids, and peritrochoids. More recently this was recognized in 1894 and proposed using just “trochoids” [12] even though this term is often restricted to the case where a circle rolls along a line. More recently the term “centered trochoid” has been proposed [3]. We shall use *central trochoid* and use the term *central cycloid* to denote a hypocycloid, epicycloid, or pericycloid. The central cycloids are those central trochoids that have cusps.

Although the curves generated by epicyclic motion are central trochoids the deferent and

epicycle are generally not the same as the fixed and rolling circles in the roulette construction. However the fixed circle can be concentric with the deferent and at any moment in time the rolling circle can be concentric with the epicycle. Only the radii may need to be different.

To determine the correct radii for the fixed and rolling circles we make use of the no slip condition. The rolling circle may not slip as it goes around the fixed circle. This means that the instantaneous velocity of the contact point is the zero vector $(0, 0)^T$. For epicyclic motion there is exactly one point, at any given moment in time, that is instantaneously at rest so this must be where the contact point for the fixed and rolling circles are at that moment.

The contact point of any pair of tangent circles is collinear with their centers and by convention their centers are on the x -axis at $t = 0$ so at this time the contact point is on the x -axis as well. We let a denote the x -coordinate of the contact point at time $t = 0$. So $|a|$ is the radius of the fixed circle.

At $t = 0$ the vector $(r_1, 0)^T$ is rotating with angular velocity ω_1 about $(0, 0)^T$ while the vector $(a, 0)^T - (r_1, 0)^T$ is rotating with angular velocity ω_2 about $(r_1, 0)^T$. Taking the derivative with respect to time, evaluating at $t = 0$, and setting the result equal to the zero vector gives

$$\begin{pmatrix} 0 \\ 0 \end{pmatrix} = \omega_1 R_{\pi/2} \begin{pmatrix} r_1 \\ 0 \end{pmatrix} + \omega_2 R_{\pi/2} \left(\begin{pmatrix} a \\ 0 \end{pmatrix} - \begin{pmatrix} r_1 \\ 0 \end{pmatrix} \right)$$

which has the unique solution $a = (1 - \omega_1/\omega_2)r_1$ (since $\omega_2 \neq 0$). To get the radius of the rolling wheel we set $b = a - r_1$, i.e. the directed distance from the center of the rolling circle to the contact point. The radius of the rolling circle is $|b|$.

The center of the fixed circle is at $(0, 0)^T$ and at $t = 0$ the center of the rolling circle is at $(r_1, 0)^T$. If $\omega_1/\omega_2 < 0$ then $r_1 < a$, the contact point is on the right hand side of both circles, and the fixed circle is outside of the rolling circle. So the curve is a hypotrochoid (see figure 3). If $0 < \omega_1/\omega_2 < 1$ then $0 < a < r_1$, the contact point is between the circles, and the circles are externally tangent. So the curve is an epitrochoid. If $1 < \omega_1/\omega_2$ then $a < 0$, the contact point is on the left hand side of both circles,

and the fixed circle is inside of the rolling circle. So the curve is a peritrochoid.

From these facts the usual parameterizations for the central trochoids in terms of the radii $|a|$, $|b|$ and the angle $\phi = \omega_1 t$ can easily be derived. It is convenient to work with (3.1) because each of the epicyclic parameters occurs just once in the expression. It is helpful to keep in mind, though, the different ways that central trochoids can be constructed, *e.g.* either by epicyclic motion or as a roulette.

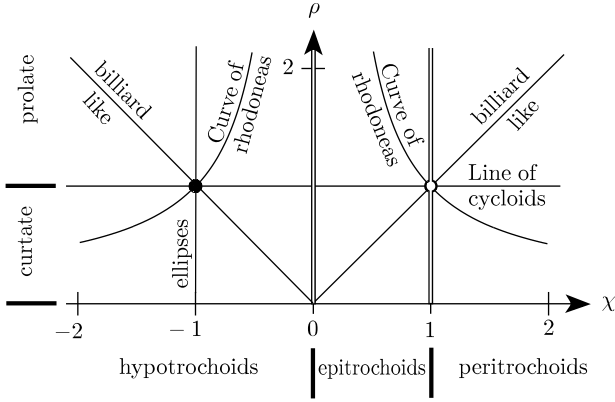


Figure 4: The spaces of hypotrochoids, $\overline{\mathcal{H}}$, of epitrochoids, $\overline{\mathcal{E}}$, and of peritrochoids, $\overline{\mathcal{P}}$. Along with the four distinguished cases, central cycloids, ellipses, billiard like, and rhodoneas.

We are primarily concerned with the shape of the central trochoids rather than their position, orientation, or size. So we will determine the space of similarity classes of central trochoids. For this purpose we introduce two geometrically invariant parameters for the central trochoids.

One commonly used geometric invariant for describing the shape of a central trochoid is $\rho = |\omega_2/\omega_1|r_2/r_1$. This is often called the *arm ratio*. This is because the line segment connecting the center of the rolling circle to the tracing point is often called the *arm* and ρ is the ratio of the arm's length to the radius of the rolling circle, $r_2/|b| = \rho$. When $\rho = 0$ the resulting curve is just a single point if $\omega_1 = 0$ and a circle otherwise. We do not wish to regard these as special cases of central trochoids so we require $\rho > 0$. When $0 < \rho < 1$ the central trochoid is curtate, when $\rho = 1$ the central trochoid is a central cy-

cloid, and when $\rho > 1$ the central trochoid is prolate.

Another geometrical invariant that we will use is the ratio of angular velocities $\chi = \omega_1/\omega_2$ (recall $\omega_2 \neq 0$). We call χ the *turning ratio*. It can also be expressed as $\chi = (b/a)/(b/a - 1)$. The quantity $|b/a|$ is often called the *wheel ratio*. We will see that for curtate central trochoids the wheel ratio equals κ (for $\omega_1 > 0$).

Even with $\rho > 0$ if $\chi = 0, 1$ then the curve that is traced out is a circle which we do not wish to include as a type of central trochoid. When $\chi < 0$ the central trochoid is a hypocycloid, when $0 < \chi < 1$ the central trochoid is an epitrochoid, and when $1 < \chi$ the central trochoid is a peritrochoid (see figure 4). We set

$$\begin{aligned}\overline{\mathcal{H}} &= \{ (\chi, \rho) \mid \chi < 0, \rho > 0 \} \\ \overline{\mathcal{E}} &= \{ (\chi, \rho) \mid 0 < \chi < 1, \rho > 0 \} \\ \overline{\mathcal{P}} &= \{ (\chi, \rho) \mid 1 < \chi, \rho > 0 \}\end{aligned}$$

and $\overline{\mathcal{T}} = \overline{\mathcal{H}} \cup \overline{\mathcal{E}} \cup \overline{\mathcal{P}}$.

In addition to the central cycloids there are three other cases of central trochoids worth distinguishing. These cases also form curves in $\overline{\mathcal{T}}$ as shown in figure 4. The first of these cases is given by the vertical line $\chi = -1$. The equation for the hypotrochoid reduces to

$$\begin{pmatrix} x(t) \\ y(t) \end{pmatrix} = \begin{pmatrix} (r_1 + r_2) \cos(\omega_1 t) \\ (r_1 - r_2) \sin(\omega_1 t) \end{pmatrix}$$

which determines an ellipse with semi-major axis $r_1 + r_2$ and semi-minor axis $|r_1 - r_2|$.

We call the cases given by the diagonal lines $\rho = |\chi|$ “billiard like”. These curves have long arcs with low curvature alternating with short arcs with high curvature. They are fairly well approximated by the paths made by a frictionless billiard ball rolling on a circular table which travels along straight line segments and bounce at the table's edge.

The remaining distinguished case of central trochoids corresponds to the central trochoid passing through its own center of symmetry. The minimum radius of a central trochoid is zero if and only if the deferent and epicycle have the same size. When $r_1 = r_2$ the distance of the

κ	hypo-	epi-	peri-
prolate	$\frac{1}{\chi-1}$	$\frac{1}{1-\chi}$	$\frac{1}{\chi-1}$
curtate	$\frac{\chi}{\chi-1}$	$\frac{\chi}{1-\chi}$	$\frac{\chi}{\chi-1}$

Table 1: The value of κ for central trochoids when the rolling wheel revolves in the anticlockwise direction, $\omega_1 > 0$. For $\omega_1 < 0$ take the negative of each table entry.

tracing point from the center of the curve, as a function of time, is

$$2r_1 \cos(((\omega_1 - \omega_2)/2) t)$$

which is essentially the defining condition for “rhodonea” curves³. The condition $r_1 = r_2$ is equivalent to $\rho|\chi| = 1$ which specifies a pair of hyperbolic arcs in $\overline{\mathcal{T}}$ (see figure 4). These hyperbolic arcs form the subspace of rhodonea curves. Below the hyperbolic arcs the deferent is larger than the epicycle while above the hyperbolic arcs the deferent is smaller than the epicycle.

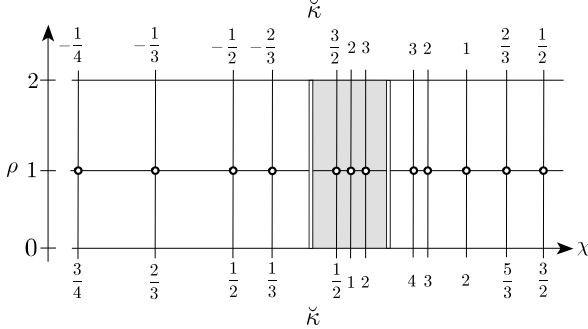


Figure 5: The isogonal curves in $\overline{\mathcal{T}}$ are vertical line segments. They are labeled with their value for κ . The value of κ changes by ± 1 when the line of cycloids is crossed. The region in $\overline{\mathcal{E}}$ is shaded to facilitate comparison to figure 4.

In $\overline{\mathcal{H}}$ the sets of hypocycloids, ellipses, billiard like curves, and rhodoneas all intersect at one point $(\chi, \rho) = (-1, 1)$. This particular special case is known as the “Tusi couple”⁴. For the Tusi couple the tracing point goes back and

forth along a line segment. For the Tusi couple the tangent vector is undefined at the end points of the line segment, as with the cusps of central cycloids. The line segment can be regarded as a degenerate ellipse. The line segment is literally a billiard curve for a round table so we can say it is a billiard like curve that passes through its center of symmetry.

The Tusi couple is the only instance in which the curvature of a central trochoid is zero at any point. Hence central trochoids do not have inflection points.

The value of κ for central trochoids can be computed from equation (2.2). It almost reduces to an uncomplicated function of χ except that it depends on the signs of ω_1 , $\rho - 1$, and $\chi(\chi - 1)$. The formulas for κ are shown in table 1. For any real number except zero there is a central trochoid whose value for κ is the given real number.

Combining $\chi = (b/a)/(b/a - 1)$ with $\kappa = \chi/(\chi - 1)$ gives $\kappa = b/a$. So we see from table 1 that $\kappa = b/a$ for curtate hypotrochoids and peritrochoids. For curtate epitrochoids $\kappa = -b/a$. The signs of a , b are the same for hypotrochoids and peritrochoids and opposite for curtate epitrochoids. Therefore the total turning number for a periodic arc of a curtate central trochoid is the same as the wheel ratio, *i.e.* $\kappa = |b/a|$.

The isogonal curves in $\overline{\mathcal{T}}$ are vertical line segments which span the heights of the curtate and prolate regions. When the line of central cycloids is crossed the value of κ changes by ± 1 (see figure 5). The central trochoids undergo a cusp transition. In this transition a loop is either added or removed from each periodic arc of the central trochoid.

A sufficient, but not necessary, condition for two central trochoids to be similar is for them to have the same values for χ and ρ . We will obtain the spaces of similarity classes of central trochoids by quotienting each of the spaces $\overline{\mathcal{H}}$, $\overline{\mathcal{E}}$, and $\overline{\mathcal{P}}$.

In models for the planetary motion the epicycle was generally much smaller than the deferent. Actually though, because vector addition is commutative, it doesn’t matter which of the two circles we take to be the deferent and epicy-

³Studied by Guido Grandi around 1723

⁴Studied by Nasir al-Din al-Tusi around 1247

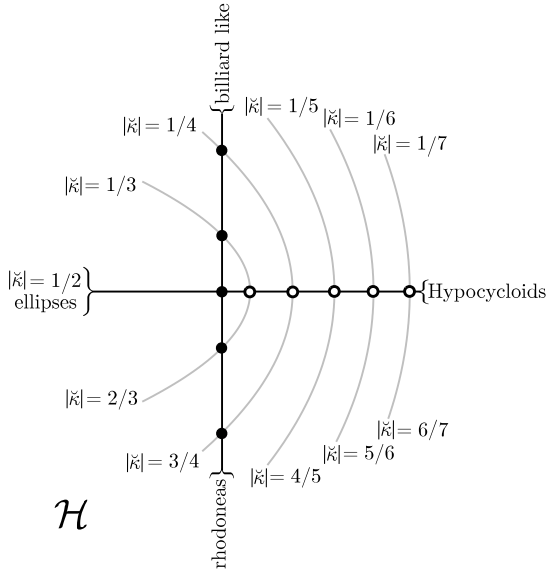


Figure 6: The space, \mathcal{H} , of similarity classes of Hypotrochoids. The origin corresponds to the Tusi couple. The four compass directions correspond to the four distinguished cases. The isogonal curves are shown in gray and they are labeled with their $|\kappa|$ values. The value of $|\kappa|$ jumps as an isogonal curve passes through the line of hypocycloids.

cle. If we let the center of the deferent revolve about the center of the epicycle with angular velocity ω_2 while the deferent spins with angular velocity ω_1 then the exact same curve can be traced out. However when we look for fixed and rolling circles to generate the central trochoid we get a different location for the point at instantaneous rest and thus different radii for the fixed and rolling circles. This fact is known as David Bernoulli's "dual generation theorem".

A consequence of the dual generation theorem is that the ordered pair $(1/\chi, 1/\rho)$ determines the same similarity class of central trochoids as (χ, ρ) . A curtate hypotrochoid is geometrically similar to a prolate hypotrochoid and *visa versa*. A prolate epitrochoid is similar to a curtate peritrochoid and *visa versa*. A curtate epitrochoid is similar to a prolate peritrochoid and *visa versa*.

The terms "hypotrochoid", "epitrochoid", "peritrochoid", "curtate", and "prolate" do not designate geometric similarity classes of curves but

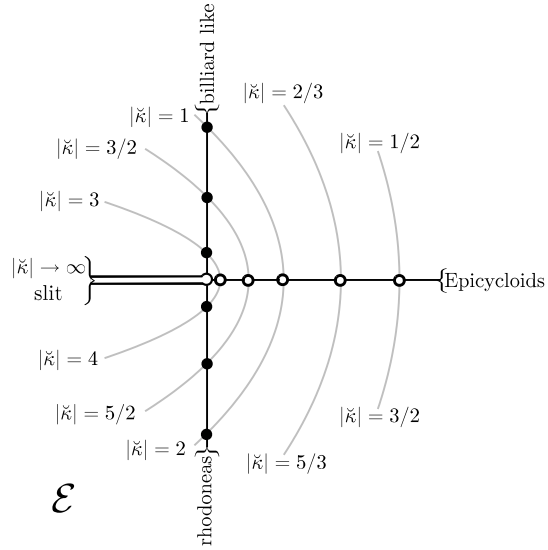


Figure 7: The space, \mathcal{E} , of similarity classes of Epitrochoids. The negative real axis and the origin make up the complement of \mathcal{E} in \mathbf{C} . The other three compass directions correspond to the three distinguished cases of Epitrochoids. The isogonal curves are shown in gray and they are labeled with their $|\kappa|$ values. The value of $|\kappa|$ jumps as the isogonal curve passes through the line of epicycloids.

merely describe how the curves can be constructed geometrically. Many geometric figures can be constructed in more than one way. This terminology can lead to some confusion particularly since peritrochoids have been regarded as epitrochoids by some authors while other authors have regarded them as hypotrochoids. Willson gives an overview on this terminology in the appendix to his 1898 book [18].

Every central trochoid, except for central cycloids, can be constructed as a curtate central trochoid and as a prolate central trochoid. The value of $|\kappa|$ equals the wheel ratio in the curtate method of construction. We can think of κ as a generalization of the wheel ratio to other types of curves with periodically varying curvature. Although κ can equal 0 for some curves with periodically varying curvature but not for central trochoids.

Suppose we have two central trochoids with parameters $\omega_1, \omega_2, r_1, r_2$ and $\omega'_1, \omega'_2, r'_1, r'_2$. A

necessary condition for two central trochoids to be similar is for the ratio of their minimum radius to their maximum radius be the same, *i.e.*

$$\frac{|r_1 - r_2|}{r_1 + r_2} = \frac{|r'_1 - r'_2|}{r'_1 + r'_2}$$

Since the radii are positive this equation is equivalent to the equation

$$\left(\frac{r'_1}{r'_2} - \frac{r_1}{r_2}\right) \left(\frac{r'_1}{r'_2} - \frac{r_2}{r_1}\right) = 0$$

If $r'_1/r'_2 = r_1/r_2$ then its necessary for $\omega'_1/\omega'_2 = \omega_1/\omega_2$ and if $r'_1/r'_2 = r_2/r_1$ then its necessary for $\omega'_1/\omega'_2 = \omega_2/\omega_1$. Therefore the only points in $\overline{\mathcal{T}}$ that correspond to the same similarity class as (χ, ρ) is $(1/\chi, 1/\rho)$.

We denote the space of similarity classes of hypotrochoids by \mathcal{H} . To denote the members of \mathcal{H} we use the term *Hypotrochoid* with the first letter capitalized. The word “hypotrochoid” with all lower case letters describes how the curve was constructed. For $(\chi, \rho) \in \overline{\mathcal{H}}$ the function

$$(\chi, \rho) \mapsto (\log(-\chi) + i \log(\rho))^2$$

is onto the complex plane, \mathbf{C} , and it is two to one everywhere except at the Tusi couple. The point with the same image as (χ, ρ) is $(1/\chi, 1/\rho)$ so we can identify \mathcal{H} with \mathbf{C} (see figure 6).

The value of χ is negative for hypotrochoids so regardless of whether it is prolate or curtate $-1 < \kappa < 1$. The projection from $\overline{\mathcal{H}}$ to \mathcal{H} maps the isogonal curves with $\kappa = \pm 1/2$ to the line of ellipses. Otherwise it maps pairs of isogonal curves with opposite sign to the same semiparabolic arc in \mathcal{H} . We can associate the value of $|\kappa|$ to each semiparabolic arc. The semiparabolic arcs whose values for $|\kappa|$ sum to 1 form the entire parabola except for its vertex on the line of Hypocycloids.

We denote the space of similarity classes of epitrochoids by \mathcal{E} . For members of \mathcal{E} we use the term *Epitrochoid* with the first letter capitalized. The words “epitrochoid” and “peritrochoid” with all lower case letters describes how the curve was constructed. For $(\chi, \rho) \in \overline{\mathcal{E}} \cup \overline{\mathcal{P}}$ the function

$$(\chi, \rho) \mapsto (\log(\chi) + i \log(\rho))^2$$

is onto the complex plane \mathbf{C} minus the non-positive real axis. It is two to one everywhere in $\overline{\mathcal{E}} \cup \overline{\mathcal{P}}$. The point with the same image as (χ, ρ) is $(1/\chi, 1/\rho)$ so we can identify \mathcal{E} with the slitted complex plane (see figure 7).

The value of χ is positive for an epitrochoid or peritrochoid (for $\omega_1 > 0$) so regardless of whether it is prolate or curtate $\kappa > 0$. The projection from $\overline{\mathcal{E}}$ to \mathcal{E} maps pairs of isogonal curves with the same κ value to the same semiparabolic arc in \mathcal{E} . To obviate the issue of how the Epitrochoids are parameterized we associate the value of $|\kappa|$ to each semiparabolic arc. If the difference in $|\kappa|$ between a semiparabolic arc in the lower half-plane of \mathcal{E} and a semiparabolic arc in the upper half-plane of \mathcal{E} is 1 then their union is the entire parabola except for its vertex on the line of Epicycloids.

Example 2 - The spherical pendulum

The spherical pendulum is an idealized mechanical system. It is comprised of a weightless inextensible *rod*, essentially a line segment with length ℓ . One end of the rod, the *pivot*, is motionless for all time. The other end, the *bob*, is the location of a point particle with mass m . The bob is constrained to move on a sphere of radius ℓ centered at the pivot while subjected to a uniform gravitational field with strength g .

We take the pivot to be the origin of a Cartesian coordinate system for the spherical pendulum. We take the direction of the gravitational field to be the negative direction of the z -axis. The z -axis is also called the *pendulum's axis*. The plane through the pivot and orthogonal to the pendulum's axis is the *support plane*. The support plane contains the (x, y) -axes of the coordinate system (see figure 8). Because the spherical pendulum is symmetrical about its axis the orientation of the (x, y) -axes is completely arbitrary.

We also use spherical coordinates to specify the position of the bob. Because the letters θ, φ are used through out this article to describe the direction of the velocity along planar curves we let ϑ stand for the polar angle of the spherical coordinate system and ψ stand for the azimuthal angle (see figure 8).

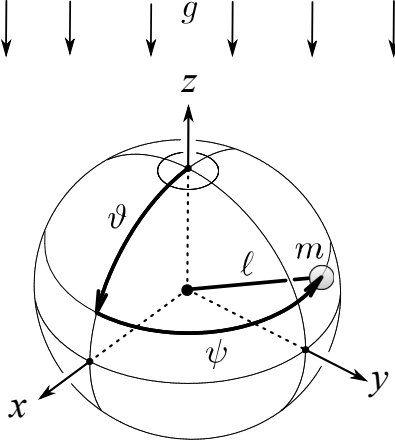


Figure 8: Cartesian coordinates, (x, y, z) , and spherical coordinates, (ϑ, ψ) for the bob of a spherical pendulum. They are related by $(x, y, z) = \ell (\sin(\vartheta) \cos(\psi), \sin(\vartheta) \sin(\psi), \cos(\vartheta))$.

The theory presented in section 2 can be generalized to curves on a sphere using the concept of geodesic curvature but to avoid unnecessary complications in this example we will study the path of the bob from a bird's eye view. More precisely stated we orthogonally project the bob's path on the sphere into the support plane. We treat the spherical pendulum as merely a mechanism for generating planar curves which are the objects of our study here.

We present a short review of the spherical pendulum's dynamics. The bob moves in three dimensional space but it is subject to a single holonomic constraint so it has two degrees of freedom. Two independent integrals of motion are the total energy or Hamiltonian, H and the vertical component of its angular momentum, J . The system is fully integrable. Its orbits are either quasiperiodic, periodic, or fixed points.

The projection of the bob's position to the pendulum's axis is always periodic. When the bob's z -coordinate has a minimal period it is sometimes referred to as the *pendulum's period* even if the pendulum is behaving quasiperiodically. So long as $J \neq 0$ the bob's (x, y) coordinates will be rotated about the pendulum's axis by a nonzero amount during the pendulum's period. Typically the angle for this rotation is irrational so the overall motion and its projection

to the support plane is quasiperiodic. It will be shown that the pendulum's period is the common minimal period of $v(t)$, $\kappa(t)$ for the (x, y) -curves so we can apply the theory from section 2.

The kinetic energy of the bob is

$$\frac{1}{2}m(\dot{x}^2 + \dot{y}^2 + \dot{z}^2) = \frac{1}{2}m\ell^2(\dot{\vartheta}^2 + \sin^2(\vartheta)\dot{\psi}^2)$$

and the potential energy is $U = mgz = mg\ell \cos(\vartheta)$. Since U is independent of $\dot{\vartheta}$ and $\dot{\psi}$ the conjugate momenta are

$$\begin{aligned} P_{\vartheta} &= \frac{\partial}{\partial \dot{\vartheta}} \frac{1}{2}m\ell^2(\dot{\vartheta}^2 + \sin^2(\vartheta)\dot{\psi}^2) = m\ell^2\dot{\vartheta} \\ J &= \frac{\partial}{\partial \dot{\psi}} \frac{1}{2}m\ell^2(\dot{\vartheta}^2 + \sin^2(\vartheta)\dot{\psi}^2) = m\ell^2 \sin^2(\vartheta)\dot{\psi} \end{aligned}$$

These are the horizontal and vertical components of the bob's total angular momentum respectively. The state of the spherical pendulum is completely specified by the canonical variables $(\vartheta, P_{\vartheta}, \psi, J)$. The Hamiltonian is

$$H(\vartheta, P_{\vartheta}, \psi, J) = \frac{1}{2m\ell^2} \left(P_{\vartheta}^2 + \frac{J^2}{\sin^2(\vartheta)} \right) + mg\ell \cos(\vartheta) \quad (3.2)$$

The fact that H is independent of ψ shows us that the value of J is constant. Although the state space is four dimensional the dynamics can be reduced to two dimensions because H , J are constant. Moreover the reduced system has a nondimensionalized form. Physically, the parameters, m , g , ℓ , are limited to positive values and varying them does not produce any qualitative changes in behavior so long as they remain positive. To obtain the reduced system we nondimensionalized the constants of motion, we define a dimensionless potential energy and its dimensionless rate of change, and we define a dimensionless time:

$$\begin{aligned} (h, j) &= \left(\frac{H}{mg\ell}, \frac{J}{m\ell\sqrt{g\ell}} \right) \\ (u, w)^T &= \left(\frac{U}{mg\ell}, \sqrt{\frac{\ell}{g}} \dot{u} \right)^T \\ \mathbf{t} &= \sqrt{g/\ell} t \end{aligned}$$

The equations of motion which can be obtained from the Hamiltonian (3.2) can be used to show

that $(u, w)^T$ satisfies the differential equation

$$\begin{pmatrix} du/dt \\ dw/dt \end{pmatrix} = \begin{pmatrix} w \\ 3u^2 - 2hu - 1 \end{pmatrix} \quad (3.3)$$

This is known as the *reduced system* for the spherical pendulum. Its is not a straight forward initial value problem. First of all the initial value for u must be in the interval $[-1, 1]$. Secondly it follows from (3.2) that

$$h = \frac{1}{2} \frac{w^2 + j^2}{1 - u^2} + u \quad (3.4)$$

Although $(u, w)^T$ varies with time the value of h depends on $(u, w)^T$ in such a way that it does not change with time. The value of h can be determined by (3.4) from the initial value for $(u, w)^T$ and the constant value for j . Once the value of h has been determined from the initial conditions it can be treated as a fixed parameter in (3.3).

The (x, y) -curves can be obtained from a solution for u by using a single quadrature.

$$\begin{aligned} \psi(t) &= \psi(0) + j \int_0^{\sqrt{g/\ell} t} \frac{d\tau}{1 - u(\tau)^2} \\ \begin{pmatrix} x(t) \\ y(t) \end{pmatrix} &= \ell \sqrt{1 - u(t)^2} \begin{pmatrix} \cos(\psi(t)) \\ \sin(\psi(t)) \end{pmatrix} \end{aligned} \quad (3.5)$$

The maximum potential energy is attained when the bob is directly above the pivot and the minimum potential energy is attained when the bob is directly below the pivot. If the bob has no kinetic energy when its directly above or below the pivot then it will remain where it is. These two states are the fixed points of the Hamiltonian system (3.2). If $h = -1$ then the bob must be motionless directly below the pivot. This is the minimum possible value for h . There is no limit to how fast the bob can move so h has no upper bound.

For each $h \geq -1$ there is a finite range of values for j . The extreme values for j can be obtained by rearranging (3.4) to

$$-\frac{1}{2} j^2 = \frac{1}{2} w^2 - (h - u)(1 - u^2) \quad (3.6)$$

and differentiating the right hand side with respect to u and w while treating h as a fixed parameter. There is one critical point for j which

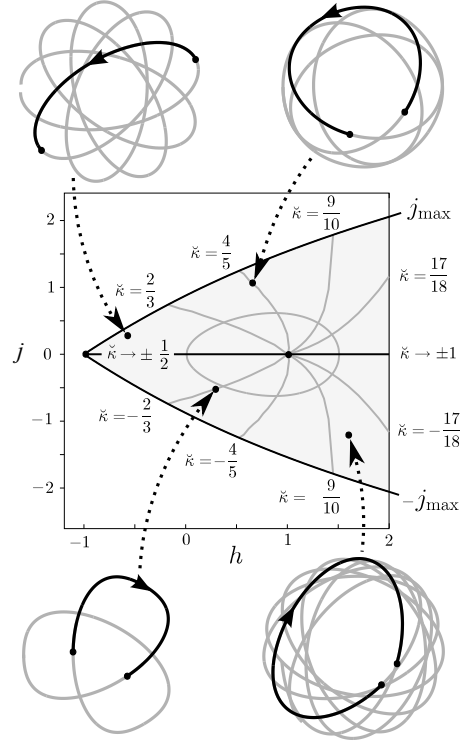


Figure 9: The energy-momentum space, \mathcal{P} , for the spherical pendulum is the light gray region bounded by the black $\pm j_{\max}$ curves. The isogonic curves, shown in dark gray, are labeled with their values for κ . They radiate from $(1, 0)$. The dark gray oval, $27j^2 = 2h(9 - 4h^2)$, is where inflection points partition the corresponding (x, y) -curves into periodic arcs. Outside of the oval the (x, y) -curves do not have inflection points. Insets show (x, y) -curves in gray each with a periodic arc shown in black. Dotted arrows point to the corresponding (h, j) values.

is $((h - \sqrt{h^2 + 3})/3, 0)^T$. The maximum value for j is

$$j_{\max} = \frac{2}{9} \sqrt{3 ((h^2 + 3)^{3/2} - h^3 + 9h)}$$

and the minimum value is $-j_{\max}$. The graph of j_{\max} is an increasing, concave down, curve with a single end point as shown in figure 9. The set of all possible values for (h, j) is the *energy-momentum space* for the spherical pendulum,

$$\mathcal{P} = \{ (h, j) : h \geq -1, |j| \leq j_{\max} \}$$

For $j = 0$ the angular velocity $\dot{\psi}$ is always zero and the pendulum moves within a vertical

plane. In this case it is often called a *planar pendulum* even though there are no physical forces constraining it within a plane. If $(h, j) = (-1, 0)$ the (x, y) -curve is just a point. If $(h, j) = (1, 0)$ the bob can be directly above the pivot or it can move asymptotically towards that position. For each h such that $h > -1$ and $h \neq 1$ all of the (x, y) -curves corresponding to $(h, 0)$ are line segments with the same length.

The right hand side of (3.6) can be taken as a Hamiltonian function for the reduced system (3.3). Thus the critical point of j corresponds to a fixed point of the reduced system. So the extreme values for j are attained when $w = 0$, *i.e.* the potential energy is constant. In these cases the height of the bob does not change. This is often referred to as a *conical pendulum* because the rod sweeps out a cone. The bob rotates along a horizontal circle with the sign of j determining the direction of rotation. For each $h > -1$ all of the (x, y) -curves determined by $(h, \pm j_{\max})$ are the same circle.

For each (h, j) in

$$\mathcal{R} = \{ (h, j) : h > -1, 0 < |j| < j_{\max} \}$$

the subset of the spherical pendulum's state space which is mapped to (h, j) is a torus⁵ [2]. The action of the group of rotations about the pendulum's axis can be extended to the whole state space of the pendulum and for each $(h, j) \in \mathcal{R}$ the corresponding torus is invariant under this action. Rotations about the pendulum's axis have no effect on w and these tori can be projected into a three dimensional space while preserving their symmetry by using the coordinates (x, y, w) (see figure 10). For each $(h, j) \in \mathcal{R}$ all of the corresponding (x, y) -curves are rotated copies of each other. The orbits typically wind quasiperiodically around the torus but they can be periodic. In either case the curvature of the (x, y) -curve varies periodically. The value of κ is defined for the corresponding (x, y) -curve if and only if $(h, j) \in \mathcal{R}$.

Since the shape of the (x, y) -curves is completely determined by $(h, j) \in \mathcal{R}$ we can think of κ as a function on the space \mathcal{R} . We let T denote

⁵Cushman's \mathcal{R} space is a little larger than this.

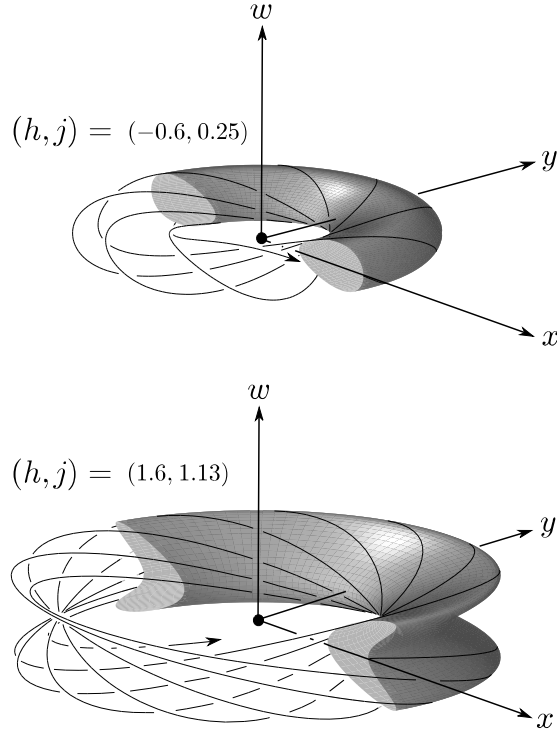


Figure 10: The projection of the invariant tori corresponding to given (h, j) values into the coordinate space for (x, y, w) . The location of the (h, j) values in \mathcal{P} is shown in figure 9. Each torus shows the projection of a rotationally symmetric quasiperiodic orbit in the torus.

the period of the reduced system in dimensionless time \mathbf{t} . T depends on (h, j) . In physical time t the period is $\sqrt{\ell/g} T$. We obtain the velocity of the (x, y) -curves from (3.5) and (3.6).

$$v = \sqrt{g\ell(2h - 2u - w^2)}$$

The period of $2h - 2u - w^2$ is the same as the period of the reduced system and since the expression under the radical is positive for all time for $(h, j) \in \mathcal{R}$ the period of v is the same as the period of the reduced system. We also obtain the curvature from (3.5) and (3.6).

$$\kappa = \frac{\dot{x}\ddot{y} - \dot{y}\ddot{x}}{v^3} = j\sqrt{g^3\ell} \frac{2h - 3u}{v^3}$$

which has the same period. From equation (2.2) and the change of variables theorem we get an expression for κ entirely in terms of the reduced

system.

$$\tilde{\kappa} = \frac{j}{2\pi} \int_0^T \frac{2h - 3u}{2h - 2u - w^2} d\tau \quad (3.7)$$

A few numerically computed isogonal curves in \mathcal{R} are shown in figure 9. The isogonal curves radiate from the point $(h, j) = (1, 0)$.

It is common to approximate the behavior of the spherical pendulum when (h, j) is near the vertex $(-1, 0) \in \mathcal{P}$ by linearizing the system about its fixed point for $(h, j) = (-1, 0)$. In this case we might expect that the (x, y) -curves for the spherical pendulum could be well approximated by Lissajous curves since we are projecting the state variables to the position variables (x, y) . However because the spherical pendulum is symmetrical about its axis the two frequencies of the linearized system are equal and therefore, regardless of the initial conditions, the only type of Lissajous curves generated by projecting the state variables of the linearized system to the position variables are ellipses or line segments. Furthermore the eigenvalues of the linearized system are purely imaginary so the Hartman-Grobman theorem does not apply [5], *i.e.* there need not be a neighborhood in which the spherical pendulum is equivalent to its linearization. The spherical pendulum is in fact highly nonlinear [11]. No matter how close $(h, j) \in \mathcal{R}$ is to $(-1, 0)$ the (x, y) -curves resemble Hypotrochoids more than they do Lissajous curves (see insets in figure 9), which is not too surprising given the geometry of the spherical pendulum.

It is interesting to compare the spaces \mathcal{P} and \mathcal{R} (figure 9) with the spaces $\overline{\mathcal{H}}$ (figure 5) and \mathcal{H} (figure 6). For these spaces the reflection about the horizontal axis maps isogonal curves to isogonal curves and the range of observed values for $\tilde{\kappa}$ is in the open interval $(-1, 1)$. Also in these spaces the range of observed values for $|\tilde{\kappa}|$ below the horizontal axis is the open interval $(1/2, 1)$.

Numerical analysis indicates that in \mathcal{R} the value of $|\tilde{\kappa}|$ can be within any tiny distance above $1/2$ but it can not be $1/2$ or less. For $h \in (-1, 1)$ the value of $\tilde{\kappa}$ appears to converge to $1/2$ as j approaches 0 from above while it appears to converge to $-1/2$ as j approaches 0 from below. Numerical analysis also indicates that the value of

$|\tilde{\kappa}|$ can be within any tiny distance below 1 but it can not be 1 or more. For $h > 1$ the value of $\tilde{\kappa}$ appears to converge to 1 as j approaches 0 from above while it appears to converge to -1 as j approaches 0 from below. As (h, j) crosses the horizontal axis of \mathcal{P} the (x, y) -curves transition by collapsing to a line segment.

In $\overline{\mathcal{H}}$ the value of $\tilde{\kappa}$ converges to $1/2$ as (χ, ρ) approaches the Tusi couple, $(-1, 1)$, from below and it converges to $-1/2$ as (χ, ρ) approaches the Tusi couple from above. As (χ, ρ) crosses the Tusi couple the (x, y) -curves transition by collapsing to a line segment.

In \mathcal{P} there is a half-line for which the corresponding (x, y) -curves are line segments while in $\overline{\mathcal{H}}$ there is a single point for which the (x, y) -curves is a line segment. On the other hand in \mathcal{P} the isogonal curves radiant from a single point while in \mathcal{H} all of the isogonal curves pass through a half-line.

There are some important differences between in \mathcal{P} and \mathcal{H} . The value of $\tilde{\kappa}$ for billiard like Hypotrochoids must be in the interval $[-1/2, 1/2]$ so the (x, y) -curves generated by the spherical pendulum do not resemble billiard like Hypotrochoids. They also do not resemble rhodonea curves since they only pass through their center of symmetry when they collapse to line segments. And unlike Hypotrochoids an (x, y) -curve for the spherical pendulum can have inflection points. This happens when (h, j) is inside the oval shown in figure 9.

The value of $\tilde{\kappa}$ is associated with the intrinsic precession of the spherical pendulum. The motion of the projected image of the bob in the support plane can be thought of as a compound motion of a point around an ellipse with the rotation of the ellipse about its center. The *intrinsic precession* of the spherical pendulum is the rotation of the ellipse.

It should be briefly pointed out that the intrinsic precession of a spherical pendulum is distinct from Foucault precession. The difference was recognized by Foucault himself. As is well known, Foucault designed and built a spherical pendulum in 1851 to measure the rotation of the Earth [9]. Foucault's pendulum was designed to be set librating within a vertical plane. Since the

pendulum's support is rotating with the Earth the plane of libration appears to rotate relative to the ground below it. This motion is called *Foucault precession*.

Foucault found that it can be difficult to start a spherical pendulum with sufficiently little angular momentum so that it will appear to oscillate within a vertical plane. Even a small amount of angular momentum led to an intrinsic precession comparable to the Foucault precession. To overcome this apparent "instability" he designed his pendulum with very large m and ℓ .

If $|j|$ is small enough the periodic arcs of the (x, y) -curve generated by the spherical pendulum can be fairly well approximated by the periodic arcs of an ellipse (see top left inset in figure 9). The approximating ellipse turns in the same direction as the bob so the total curvature of a periodic arc of the (x, y) -curve of the spherical pendulum is the sum of the total curvature of a periodic arc of the approximating ellipse with the intrinsic precession of the approximating ellipse. For any nondegenerate ellipse the value of the total curvature of a periodic arc is $\check{\kappa} = \pm 1/2$ (recall figure 6). The amount of intrinsic precession that occurs during the pendulum's period is

$$\begin{cases} \check{\kappa} - 1/2 & \text{for } \check{\kappa} > 1/2 \\ \check{\kappa} + 1/2 & \text{for } \check{\kappa} < -1/2 \end{cases}$$

If $|j|$ is large the periodic arcs of the (x, y) -curve are not well approximated by periodic arcs of an ellipse (see bottom left inset in figure 9). In these cases it is not very helpful to think of the (x, y) -curve as being generated by a precessing ellipse.

The value of $\check{\kappa}$ is defined for all $(h, j) \in \mathcal{R}$ regardless of how poorly the periodic arcs of an (x, y) -curve can be approximated by the periodic arcs of an ellipse. The value of $\check{\kappa}$ tells us how far the (x, y) -curve turns during the pendulum's period as well as providing us with information about the symmetry of the (x, y) -curve.

4 Dissipative examples

In this section we consider two related models for natural systems that generate curves with peri-

odic curvature. These are the Shenoy-Rutenberg model for the paths taken by the bacterium *Listeria monocytogenes* in eukaryotic cells [6] and the Barkley-Kevrekidis model for the meander of spiral waves in excitable media such as the BZ reaction [1].

Example 3 - Actin based motility

L. monocytogenes transport themselves in eukaryotic cells by catalyzing the polymerization of the cytoskeletal protein actin. This method of propulsion can result in a bacterium following a complicated path within the cytosol at a fairly constant speed. The curvature of the paths tends to vary periodically with time so the curvature and speed have a common minimal period and we can apply the theory from section 2.

Recall from section 2 that the velocity's orientation is $\varphi(t) = \bar{\kappa} t + \tilde{\varphi}(t)$ where $\tilde{\varphi}(t)$ is periodic. In the Shenoy-Rutenberg model $\tilde{\varphi}(t) = (\Omega/\omega_0) \sin(\omega_0 t)$ where ω_0 is the angular frequency of the bacterium's spin about its long axis and Ω is a monotonic function of the distance of the effective propulsive force from the long axis. In the model the speed of the bacterium is the constant v_0 . The common minimal period of the curvature and speed is $T = 2\pi/\omega_0$ and so $\bar{\kappa} = \omega_0 \check{\kappa}$. The points of maximal curvature occur for $t \in (2\pi/\omega_0)\mathbf{Z}$ and the points of minimal curvature occur for $t \in (\pi/\omega_0) + (2\pi/\omega_0)\mathbf{Z}$.

Since $(\Omega/\omega_0) \sin(\omega_0 t)$ is an odd function the full image of the curve has reflectional symmetry. Joining an arc over a half-period with its reflected image gives a periodic arc. For integral $\check{\kappa}$ the rest of the curve can be obtained by translating the periodic arc. For non-integral $\check{\kappa}$ the rest of the curve can be obtained by rotating the periodic arc about $(\bar{x}, \bar{y})^T$.

When the initial direction is horizontal, *i.e.* $\varphi(0) = 0$, and the starting point is at the origin, *i.e.* $(x(0), y(0))^T = (0, 0)^T$, the time parameterization for the curve is

$$\begin{pmatrix} x(t) \\ y(t) \end{pmatrix} = v_0 \int_0^t \begin{pmatrix} \cos(\omega_0 \check{\kappa} \tau + (\Omega/\omega_0) \sin(\omega_0 \tau)) \\ \sin(\omega_0 \check{\kappa} \tau + (\Omega/\omega_0) \sin(\omega_0 \tau)) \end{pmatrix} d\tau \quad (4.1)$$

There is no closed form for this integral in terms of elementary functions but we can obtain a closed form that accurately approximates it by borrowing a technique from civil engineering known as

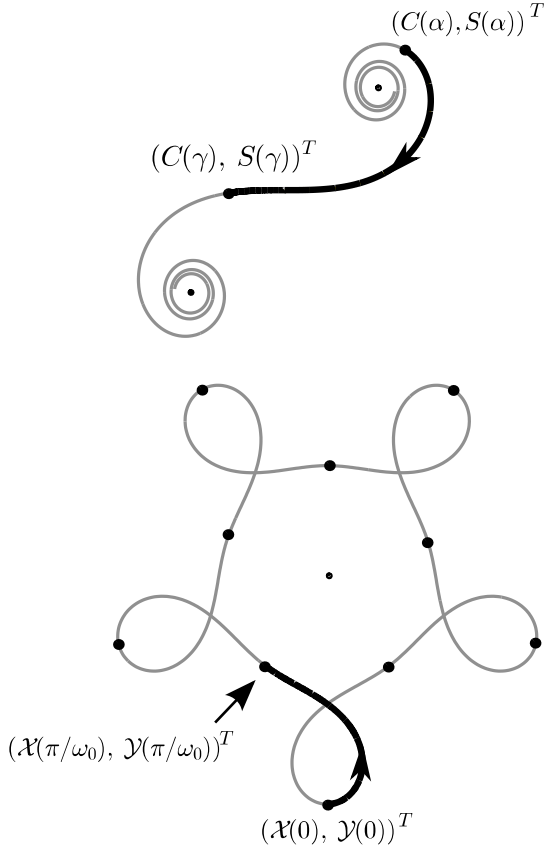


Figure 11: Generating a spiral easement approximation for an (x, y) -curve. Above: A clothoid. It is symmetrical under a half turn and the center is its unique inflection point. Below: The approximating $(\mathcal{X}, \mathcal{Y})$ -curve. The two arcs highlighted in black are geometrically similar to each other. The $(\mathcal{X}, \mathcal{Y})$ -curve can be obtained by successively reflecting its black arc about the five mirror lines shown in figure 12.

spiral easement. This technique varies the curvature of roads and train tracks in a piecewise linear fashion. For the Shenoy-Rutenberg model we approximate the curvature with the triangular wave form

$$\kappa(t) \approx \frac{\omega_0 \check{\kappa}}{v_0} + \frac{\Omega}{v_0} \left(\frac{8}{\pi^2} \arcsin(\cos(\omega_0 t)) \right)$$

This gives a piecewise quadratic approximation for $\tilde{\varphi}(t)$:

$$\frac{\Omega}{\omega_0} \left(\frac{16}{\pi^2} \arcsin(\cos(\omega_0 t/2)) \arcsin(\sin(\omega_0 t/2)) \right)$$

The rotational symmetry of the curve is unaffected by this approximation since only the $\tilde{\varphi}(t)$

term in $\varphi(t)$ is altered and the reflectional symmetry is unaffected since $\tilde{\varphi}(t)$ remains an even function. Because of the symmetry the error varies periodically and so remains bounded. The quantity

$$\left| \frac{16}{\pi^2} \arcsin(\cos(\omega_0 t/2)) \arcsin(\sin(\omega_0 t/2)) - \sin(\omega_0 t) \right|$$

is never more than 3.21° at any time. Figure 12 shows an example of a spiral easement approximation for the parametrized curve in equation (4.1)

We let $(\mathcal{X}(t), \mathcal{Y}(t))^T$ denote the time parameterization for the approximating curve to (4.1). On the interval $[0, \pi/\omega_0]$ the curvature can be written as the linear polynomial $2\beta(\alpha - \beta t)$ where

$$\alpha = \frac{\pi\omega_0\check{\kappa} + 4\Omega}{2\pi\beta v_0} \quad \beta = \frac{2}{\pi} \sqrt{\frac{\omega_0\Omega}{v_0}}$$

Integrating over a sub-interval $[0, t] \subseteq [0, \pi/\omega_0]$ gives us a closed form time parameterization for an arc of the $(\mathcal{X}(t), \mathcal{Y}(t))$ -curve,

$$\begin{pmatrix} \mathcal{X}(t) \\ \mathcal{Y}(t) \end{pmatrix} = \frac{v_0}{\beta} R_{(\alpha^2)} \begin{pmatrix} -C(\alpha - \beta t) + C(\alpha) \\ S(\alpha - \beta t) - S(\alpha) \end{pmatrix} \quad (4.2)$$

where $C(t), S(t)$ are the Fresnel trigonometric functions.

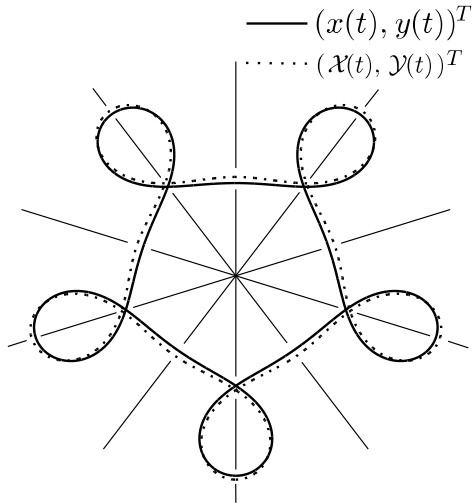


Figure 12: An (x, y) -curve with $(\check{\kappa}, \Omega/\omega_0) = (4/5, 1)$ along with its approximating $(\mathcal{X}, \mathcal{Y})$ -curve translated to have the same center. The curves' five mirror lines are also displayed.

The planar curve $t \mapsto (C(t), S(t))^T$ is known as a clothoid⁶. It is shown at the top of figure 11. It has unit speed so t is the arc length from its center, $(0,0)^T$ to $(C(t), S(t))^T$. The curvature at $(C(t), S(t))^T$ is $2t$ so every possible curvature occurs at exactly one point of the clothoid. Since the curvature is monotonic the clothoid does not intersect itself and since the curvature is unbounded in the positive and negative directions the clothoid spirals around two points.

The right hand side of equation (4.2) is the application of a odd similarity transformation to an arc of the clothoid. This approximation technique amounts to taking the extremal curvatures of the $(x, y)^T$ -curve, determining the two points on the clothoid where these extremal curvatures occur, and applying an odd similarity to the arc in the clothoid connecting the points of extremal curvature as shown in figure 11. The rest of the $(\mathcal{X}, \mathcal{Y})$ -curve is obtained by the action of the symmetry group of the $(\mathcal{X}, \mathcal{Y})$ -curve. The approximation can be further refined by translating the $(\mathcal{X}, \mathcal{Y})$ -curve so that it has the same center as the (x, y) -curve (see figure 12).

The value of $\check{\kappa}$ determines the rotational symmetry of the curve. The value of Ω/ω_0 determines the length of the clothoid arc used in approximating the curve. The effect of Ω/ω_0 for fixed $\check{\kappa}$ is perhaps best illustrated in the $\check{\kappa} = 1/2$ case (see figure 13) because there are fewer self-intersections to deal with.

As Ω/ω_0 varies the points of minimal curvature oscillate in unison along mirror lines and the points of maximal curvature oscillate in unison along mirror lines. For small Ω/ω_0 the curve has an oval shape with the points of minimal curvature closer to the center than the points of maximal curvature. As Ω/ω_0 increases the points of minimal curvature move toward the center and inflection points appear. Next the points of minimal curvature pass through the center together and then move outward. Eventually the points of minimal curvature go far from the center while the points of maximal curvature go near the center. The points of maximal

curvature pass through the center together and then proceed outward. Afterwards the points of minimal curvature pass back through the center again. The process is reminiscent of a loom except the curve becomes wound up around four points (when $\check{\kappa} = 1/2$) instead of being woven.

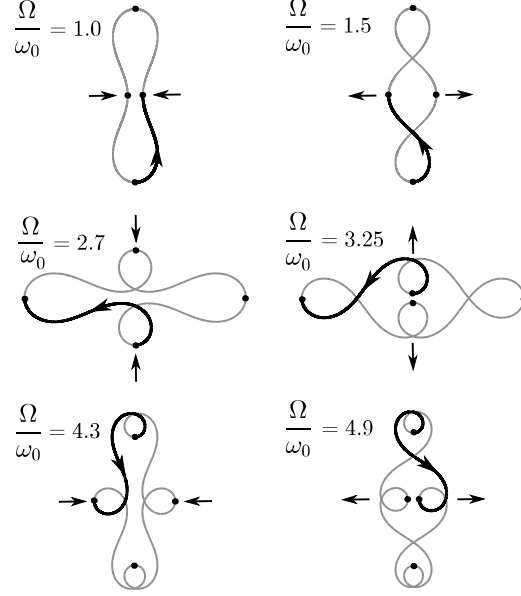


Figure 13: $(\mathcal{X}, \mathcal{Y})$ -curves with fixed $\check{\kappa} = 1/2$ and increasing Ω/ω_0 . Each row shows a pair of points with extremal curvature passing through each other at the center thereby introducing a pair of crossing points which persist as Ω/ω_0 continues to increase.

More generally, for $\check{\kappa} \notin \mathbf{Z}$, the points of maximal curvature coincide with the center if and only if $(\mathcal{X}(0), \mathcal{Y}(0))^T = (\bar{\mathcal{X}}, \bar{\mathcal{Y}})^T$ while the points of minimal curvature coincide with the center if and only if $(\mathcal{X}(\pi/\omega_0), \mathcal{Y}(\pi/\omega_0))^T = (\bar{\mathcal{X}}, \bar{\mathcal{Y}})^T$. If the points of minimal curvature coincide with the center then

$$\cos(\alpha^2) (C(\gamma) - C(\alpha)) + \sin(\alpha^2) (S(\gamma) - S(\alpha)) = 0 \quad (4.3)$$

where $\gamma = \alpha - \beta\pi/\omega_0$. This gives us a condition which must hold between $\check{\kappa}$ and Ω/ω_0 . The same condition holds if the points of maximal curvature coincide with the center except $\check{\kappa}$ is replaced with $-\check{\kappa}$. These two conditions determine two sets of curves in the $(\check{\kappa}, \Omega/\omega_0)$ parameter plane which are shown in figure 14.

These two sets of curves only intersect at integer values of $\check{\kappa}$. It turns out in these cases that

⁶ It is also known as Euler's spiral and as Cornu's spiral.

the congruence $\mathcal{G}_{\check{\kappa},T}$ reduces to the identity map, that the image of the $(\mathcal{X}, \mathcal{Y})$ -curve is closed, and that $\check{\kappa}$ is its turning number.

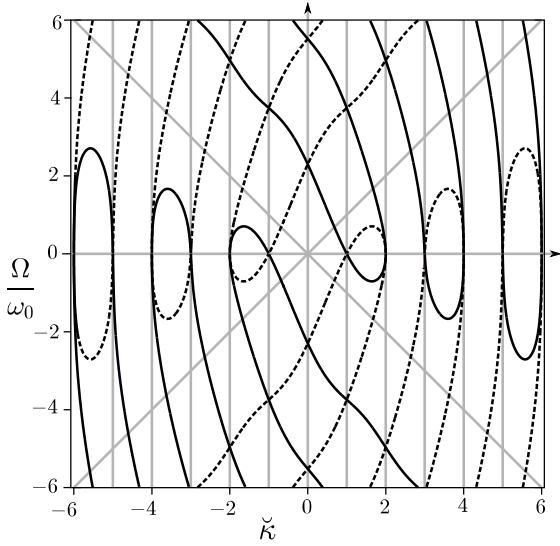


Figure 14: The parameter plane for equation (4.2) and the curves defined by (4.3). The solid black curves correspond to $(\mathcal{X}, \mathcal{Y})$ -curves whose points of minimal curvature coincide with the center. The dotted black curves correspond to $(\mathcal{X}, \mathcal{Y})$ -curves whose points of maximal curvature coincide with the center. The solid black and dotted black curves only intersect on the vertical gray lines which correspond to integer values for $\check{\kappa}$. The gray diagonal lines correspond to the appearance of inflection points in the $(\mathcal{X}, \mathcal{Y})$ -curves.

Example 4 - Spiral tip meander

Barkley's model [1] for the spiral wave tip meander can be written as the ordinary differential equation

$$\begin{pmatrix} \dot{x} \\ \dot{y} \\ \dot{\varphi} \\ \dot{v} \\ \dot{w} \end{pmatrix} = \begin{pmatrix} v \cos(\varphi) \\ v \sin(\varphi) \\ \gamma_0 w \\ v(-1/4 + (10/3)v^2 + \alpha_2 w^2 - v^4) \\ w(-1 + v^2 - w^2) \end{pmatrix}$$

Here we have replaced the variable name 's' in Barkley's equations (3) and (4) with the variable name 'v' in keeping with the convention in this article that s stands for arc length and v stands for speed.

From equation (2.2) the total curvature per periodic arc is

$$\check{\kappa} \approx \frac{\sqrt{7}\nu}{\pi} \int_0^{\sqrt{14}\pi/7} w(\tau) d\tau$$

where $\nu = \gamma_0/\sqrt{28}$. The isogonal curves for $\check{\kappa} = 1, 2, 3, 4$ are shown in figure 15 where $\mu = -(\alpha_2 + 5)/5$.

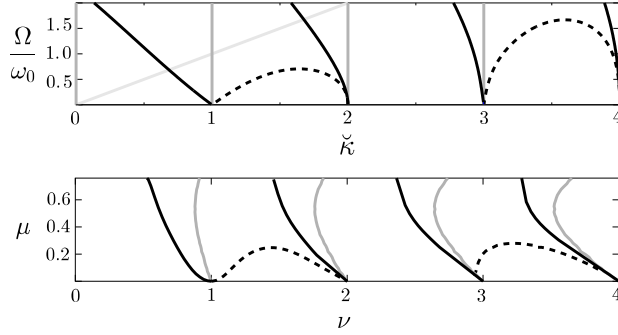


Figure 15: (Above) Blow up of a region in figure 14. (Below) The (ν, μ) parameter space for Barkley's ODE (compare to figure 3 in [1]). Curves in the two parameter spaces are depicted in the same manner as in figure 14.

5 Conclusion

References

- [1] Barkley, D. (1994). Euclidean Symmetry and the Dynamics of Rotating Spiral Waves. *Phy. Rev. Lett.*, 72(1), pp. 164–167.
- [2] Cushman, R. (1983). Geometry of the Energy Momentum Mapping of the Spherical Pendulum. *Centrum voor Wiskunde en Informatica Newsletter*, 1, 4–18.
- [3] Ferréol, R. (2015). *Trochoïde À Centre*. <http://www.mathcurve.com/courbes2d/trochoid/trochoidacentre.shtml> (accessed July 2015).
- [4] Ganguli, Surendramohan (1926). *The Theory of Plane Curves Volume II*, Second edition. University of Calcutta press.

- [5] Hartman, P. (1960), A lemma in the theory of structural stability of differential equations, *Proc. AMS*, 11, 610–620.
- [6] Hotton, S. (2010). A dynamical systems approach to actin-based motility in *Listeria monocytogenes*. *Europhys. Lett.*, 92, 30005.
- [7] Hotton, S., & Yoshimi, J. (2016). Dynamical Systems Analysis of Braitenberg Vehicles, in preparation.
- [8] Milnor, J. (1950). On the total curvature of knots. *Ann. of Math.* 52(2), pp. 248–257.
- [9] Foucault, M. L., (1851). Démonstration physique du mouvement de rotation de la terre au moyen du pendule. *C. R. Acad. Sci. Hebd Seances Acad. Sci. D*, 32 135.
- [10] Krivoruchenko, Mikhail, I., (2009). Rotation of the swing plane of Foucault’s pendulum and Thomas spin precession: Two faces of one coin. *Phys.-Usp.*, 52 821.
- [11] Malkin, I. G. (1952). Theory of stability of motion. United States Atomic Energy Commission. Washington DC.
- [12] Morely, Frank. (1894). On Adjustable Cycloidal and Trochoidal Curves. *American Journal of Mathematics*. 16(2), pp. 188–204
- [13] Olsson, M. G. (1978). The precessing spherical pendulum. *American Journal of Physics*. 46, pp. 1118–1119.
- [14] Plesser, T., & Müller, K. (1995). Fourier Analysis of the Complex Motion of Spiral Tips in Excitable Media, *International Journal of Bifurcations and Chaos*. 5(4). pp. 1071–1084.
- [15] Sullivan, J. M. (2007). Curves of Finite Total Curvature.
- [16] Van, Peter J., (1991). A Contour-Oriented Approach to Shape Analysis. Prentice Hall International.
- [17] Whitney, H., (1937). On regular closed curves in the plane. *Compositio Math.* 4. pp. 218–249.
- [18] Willson, Frederick N. (1898). Some Mathematical Curves and their Graphical Construction. MacMillan Co. New York
- [19] Winfree, A.T. (1991). Varieties of spiral wave behavior: An experimentalist’s approach to the theory of excitable media. *Chaos*, 1(3), 303–334.